Original Article

Evaluation of image quality of diffusion weighted readout segmentation of long variable echo-trains MR pulse sequence for lumbosacral nerve imaging at 3T

Osamah M. Abdulaal[1,2], Peter J. MacMahon[3,4], Louise Rainford[2], Andrea Cradock[2], Dearbhail O'Driscoll[3], Marie Galligan[2], Sultan A. Alshoabi[1], Walaa Alsharif[1], Allison McGee[2]

[1]Diagnostic Radiology Technology, College of Applied Medical Sciences, Taibah University, Madina, Saudi Arabia; [2]Diagnostic Imaging, School of Medicine, University College Dublin, Dublin, Ireland; [3]Department of Radiology, Mater Misericordiae University Hospital, Dublin, Ireland; [4]School of Medicine, University College Dublin, Dublin, Ireland

Contributions: (I) Conception and design: OM Abdulaal, A McGee, L Rainford and PJ MacMahon; (II) Administrative support: OM Abdulaal, A McGee, W Alsharif and S Alshoabi; (III) Provision of study materials or patients: OM Abdulaal, A McGee, A Cradock, M Galligan and PJ MacMahon; (IV) Collection and assembly of data: OM Abdulaal and A Cradock; (V) Data analysis and interpretation: OM Abdulaal, A McGee, D O'Driscoll, M Galligan and PJ MacMahon; (VI) Manuscript writing: All authors; (VII) Final approval of manuscript: All authors.

Correspondence to: Dr. Osamah M. Abdulaal, PhD. Assistant Professor, Diagnostic Radiology Technology, College of Applied Medical Sciences, Taibah University, Madina, Saudi Arabia. Email: oabdulaal@taibahu.edu.sa.

Background: Limited magnetic resonance (MR) pulse sequences facilitate lumbosacral nerve imaging with acceptable image quality. This study aimed to evaluate the impact of parameter modification for Diffusion Weighted Image (DWI) using Readout Segmentation of Long Variable Echo-trains (RESOLVE) sequence with opportunities for improving the visibility of lumbosacral nerves and image quality.

Methods: Following ethical approval and acquisition of informed consent, imaging of an MR phantom and twenty healthy volunteers (n=20) was prospectively performed with 3T MRI scanner. Acquired sequences included standard two-dimensional (2D) turbo spin echo sequences and readout-segmented echo-planar imaging (EPI) DWI-RESOLVE using three different b-values b-50, b-500 and b-800 s/mm^2. Signal-to-noise ratio (SNR), apparent diffusion coefficient (ADC) and nerve size were measured. Two musculoskeletal radiologists evaluated anatomical structure visualisation and image quality. Quantitative and qualitative findings for healthy volunteers were investigated for differences using Wilcoxon signed-rank and Friedman tests, respectively. Inter and intra-observer agreement was determined with κ statistics.

Results: Phantom images revealed higher SNR for images with low b-values with 206.1 (±10.9), 125.1 (±45.2) and 59.2 (±17.8) for DWI-RESOLVE images acquired at b50, b500 and b800, respectively. Comparable results were found for SNR, ADC and nerve size across normal right and left sided for healthy volunteer images. The SNR findings for b-50 images were higher than b-500 and b-800 images for healthy volunteer images. The qualitative findings ranked images acquired using b-50 and b-500 images significantly higher than corresponding b-800 images ($P<0.05$). Inter and intra-observer agreements for evaluation across all b-values ranged from 0.59 to 0.81 and 0.83 to 0.92, respectively.

Conclusions: The modified DWI-RESOLVE images facilitated visualization of the normal lumbosacral nerves with acceptable image quality, which support the clinical applicability of this sequence.

Keywords: Magnetic resonance imaging; spine; diffusion weighted imaging

Submitted Feb 26, 2022. Accepted for publication Oct 08, 2022. Published online Nov 14, 2022.
doi: 10.21037/qims-22-191
View this article at: https://dx.doi.org/10.21037/qims-22-191

Introduction

Traditionally, diffusion-weighted magnetic resonance imaging (DW-MRI) was undertaken using the single-shot echo-planar imaging (ss-EPI) sequence and was principally introduced to evaluate the central nervous system, showing high sensitivity and specificity for detecting acute infarct, tumors and abscesses (1-6). With recent hardware and software advances, DW-MRI is now in routine diagnostic use for assessment of the liver (7,8), kidneys (9) and musculoskeletal system (10).

Research suggests that DW-MRI may have an important contribution to detecting and characterizing nerve abnormalities. This scanning technique generates MR images providing information about tissue microstructure by monitoring the random movement of water molecules, which become restricted in tissues (11). A number of studies have evaluated different EPI based DWI sequences for assessing the lumbosacral nerves and found that DWI-MRI is appropriate for non-invasively assessing the lumbosacral nerves and nerve roots (12-15). However, ss-EPI DWI sequences have a number of limitations including high sensitivity to geometric distortion, signal loss and T2* blurring, mainly due to slow k-space filling in the phase encoding direction (16). Since these adverse effects are more severe at tissue boundaries, such as those involving the soft tissue, bowel gas and bone in the vicinity of the lumbosacral nerves, the associated reduction in image quality compromises the clinical usefulness of conventional ss-EPI-based DW sequences (17).

Currently, a DWI based sequence, known as Readout Segmentation of Long Variable Echo-trains (RESOLVE) involving a k-space sampling strategy in which the readout direction is divided into a number of 'readout segments', was released to improve image quality and therefore, clinical applications of DWI. This readout-segmented EPI-based DWI sequence incorporates a number of characteristics to speed up k-space traversal and thereby reduce the distortion typically associated with EPI. These include reduced echo spacing facilitated by a wide receive bandwidth, parallel imaging with generalized auto-calibrating partial parallel acquisition (GRAPPA) together with the use of an alternate k-space trajectory whereby k-space is segmented into multiple adjacent and partially overlapping segments (18). The reduction in geometric distortion achievable is proportional to the width of each segment (19). Each readout segment is acquired as a separate shot and a two-dimensional navigator-based reacquisition scheme corrects for motion-induced phase errors (16).

Literature evidence indicates that the DWI-RESOLVE sequence has applications in various anatomical regions including the brain, breast and kidney (20-23). The findings of these studies have demonstrated that through the use of shortened echo spacing in each segment and acceleration of k-space filling in the readout direction, together with parallel imaging, DWI-RESOLVE is capable of in-plane rigid motion correction and produces images with less susceptibility artifact, distortion, and blurring with higher spatial resolution than ss-EPI (20-23). This technical advancement is important to minimize the effect of artifacts that can reduce the diagnostic performance of DWI (24,25). To our knowledge, the application of the EPI DWI-RESOLVE has not been described for the lumbosacral nerves. Therefore, in this study, the DWI-RESOLVE sequence was modified and applied on a phantom to quantitatively and qualitatively establish baseline image quality characteristics on human subjects to evaluate the clarity of visualization of lumbosacral nerves and image quality in preparation for clinical study (26). We present the following article in accordance with the MDAR reporting checklist (available at https://qims.amegroups.com/article/view/10.21037/qims-22-191/rc).

Methods

Phantom construction

Ethical approval was obtained prior to commencing phantom and healthy volunteers recruitment and scanning. This research study was approved by the Research Ethics Committee at the Mater Misericordiae University Hospital, Dublin, Ireland (Reference number: 1/378/1719). The study was conducted in accordance with the Declaration of Helsinki (as revised in 2013). The phantom phase was essential to ensure that image quality is acceptable and not suffering from artifacts before performing the modified sequence on human subjects. To calculate the signal-to-noise ratio (SNR) and contrast-to-noise ratio (CNR) of images acquired using the DWI-RESOLVE MR pulse sequence, initial phantom scanning was undertaken using a cylindrical, copper sulphate-based phantom. The Perspex phantom was constructed to comprise two cylinders with the following dimensions: height 300 mm, inner diameter 185 mm and inner cylinder 140 mm fitted with a coaxial inner cylinder (inner diameter 140 mm) (*Figure 1*). The inner cylinder was filled with deionized water doped with

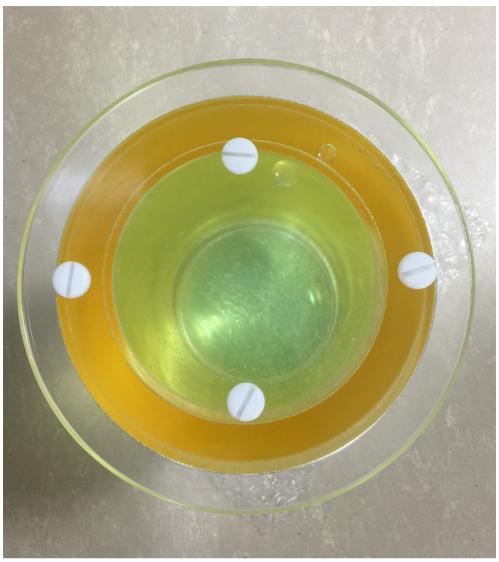

Figure 1 Image of the copper sulphate-based MR image quality phantom. The inner cylinder was filled with deionized water doped with copper sulphate and sodium chloride. The outer ring was filled with corn oil. MR, magnetic resonance.

copper sulphate (770 mg, $CuSO_4$, $5H_2O$, Sigma-Aldrich) and sodium chloride (2000 mg, NaCl, Sigma Aldrich) (27). The outer ring was filled with corn oil (Mazola®) to simulate the subcutaneous, intra-abdominal and intrapelvic fat encountered during body MR imaging (27).

Human subjects

Twenty (n=20) adult volunteers (female n=12; male n=8; age range 21-59 years; mean age 32 years; weight range 61-88 kilograms; mean weight 72.6 kilograms) were prospectively recruited and scanned over a 5-week period. Written consent form was obtained from all the participants before the MRI examinations. The healthy volunteers were medical or paramedical personnel, with no history of attending a clinician and/or physiotherapist for evaluation and/or treatment of lumbar spine disease. Any participants with contraindication according to the MR safety-screening questionnaire were excluded (28).

MR imaging protocol

Lumbosacral spine imaging was undertaken on a 3 Tesla whole-body MR system (MAGNETOM *Skyra*, Siemens Healthcare GmbH, Erlangen, Germany) with a 32-channel spinal phased array coil used together with an 18-channel body-matrix coil placed over the patient's lower abdomen/pelvis.

All participants underwent spinal MRI with both the axial 2D navigator-corrected readout-segmented EPI DWI sequence known as RESOLVE and a routine 2D MR scanning protocol for lumbar spine (*Table 1*). The high-resolution DWI-RESOLVE sequence included the following b-values: 50, 500 and 800 s/mm^2, with Spectral Attenuated Inversion Recover (SPAIR) fat suppression. The diffusion mode was 3 scan trace and monopolar diffusion scheme. The noise level for this sequence is 10 and the signal is 1. The signal is a relative term provide a guide to any changes in parameters that might compromise the SNR in the image.

Diffusion weighted gradients were applied in three directions: anteroposterior (AP), right-left (RL) and head-foot (HF). The 2D lumbar spine protocol included: sagittal T1- and T2-weighted Turbo Spin Echo (TSE), axial T2-weighted TSE of L3/L4, L4/5, and L5/S1 in a single scanning session. The conventional 2D TSE sequences were performed to ensure that the volunteer participants were not suffering from disc herniation, spinal stenosis or other unsuspected pathology.

Sequence modification

Since the DWI-RESOLVE sequence provided by the vendor (*Table 1*) was not specifically designed for evaluating the lumbosacral nerves, the sequence required modification using phantom images before applying it on human subjects. Several parameters manipulated to obtain an optimal balance between acquisition time and image quality. The selection of the b-values for the DWI-RESOLVE sequence was based on guidance from previous literature that utilized a conventional single-shot EPI-based DWI sequence for evaluating the lumbosacral nerves and nerve roots (12-14). We found that incorporating three different b-values: b-50, b-500 and b-800 s/mm^2 into the DWI-RESOLVE sequence allowed for comprehensive evaluation of the lumbosacral nerves. The b-50 images facilitated evaluation for the shape and size of nerves, while the b-500 and b-800 images enabled assessment of signal intensity differences, providing high CNR between the lumbosacral nerves and blood vessels.

The modification process involved modification of the following parameters: TR, voxel size, number of slices, field-of-view (FoV), base resolution, and bandwidth (*Table 1*).

Table 1 Scanning parameters for DWI-RESOLVE and 2D sequences

Parameters	Non-modified DWI-RESOLVE	Modified DWI-RESOLVE	Sagittal T2	Axial T2 x3	Sagittal T1
TR (ms)	5,600	12,700	3,500	2,870	650
TE (ms)	55	57	92	106	8.6
FoV read (mm^2)	230	250	280	190	280
Slice thickness (mm)	3.5	4	4	4	4
Number of slices	25	55	15	10	15
Voxel size (mm)	2.3×2.3×3.5	1.9×1.9×4	0.7×0.7×4	0.6×0.6×4	0.8×0.8×4
Base resolution	110	130	384	320	320
Phase resolution (%)	100	90	75	85	80
Phase encoding direction	AP	AP	HF	RL	HF
Phase partial Fourier	off	off	off	off	off
Echo-spacing (ms)	0.32	0.32	9.2	11.8	8.58
Bandwidth (Hz/px)	874	1012	250	252	252
PI Acceleration factor	GRAPPA-2	GRAPPA-2	GRAPPA-2	GRAPPA-2	Off
Fat suppression	SPAIR	SPAIR	NA	NA	NA
Flip angle (°)	180	180	160	160	150
Averages	1	1	1	2	1
Readout segments	7	5	NA	NA	NA
Acquisition time (mins)	7:09	10:11	2:10	1:06	3:01

DWI, diffusion weighted imaging; RESOLVE, readout segmentation of long variable echo-trains; TR, repetition time; TE, echo time; FoV, field of view; PI, parallel imaging; AP, anterior/posterior; HF, head/foot; RL, right/left; GRAPPA, generalized auto-calibrating partial parallel acquisition; SPAIR, spectral attenuated inversion recovery.

The TR was increased from 5,600 ms to 12,700 ms in order to increase the number of slices ensuring sufficient anatomical coverage. By increasing the matrix, the voxel size was reduced from 2.3 mm × 2.3 mm × 3.5 mm to 1.9 mm × 1.9 mm × 4 mm, thereby increasing spatial resolution and reducing blurring of the lumbosacral nerve roots, which require high spatial resolution to facilitate their delineation and the detection of subtle abnormalities within them (29). However, the FoV and slice thickness were increased to improve the SNR and coverage. The receive bandwidth was increased from 874 to 1,012 Hz/px to enable the TE to be minimized to support reduced acquisition time and enhanced the diffusion weighting and minimized T2 shine through (29). In an effort to reduce the acquisition time, the number of readout segments was reduced from 7 to 5. *Table 1* summarizes the changes applied to the DWI-RESOLVE sequence.

Image analysis

Quantitative assessment

Phantom: Using image J software (National Institutes of Health, Bethesda, MD, USA; http://rsbweb.nih.gov/ij), a specialist MR radiographer calculated the numerical values of MR image quality for the representative images of the phantom including: SNR and CNR. Regions of interest (ROIs) for determining the signal intensities were drawn in areas where signals from fluid and suppressed fat appeared separately in the MR images, taking care to avoid sampling signal from ghosting artifacts. The circular ROI sizes were consistent for all measurements. The ROIs were placed in the central region of the phantom. The standard deviation (SD) of the noise was measured for each image by placing a circular ROI in the background, avoiding phase ghosting or other artifacts, if present. A total of 33 images

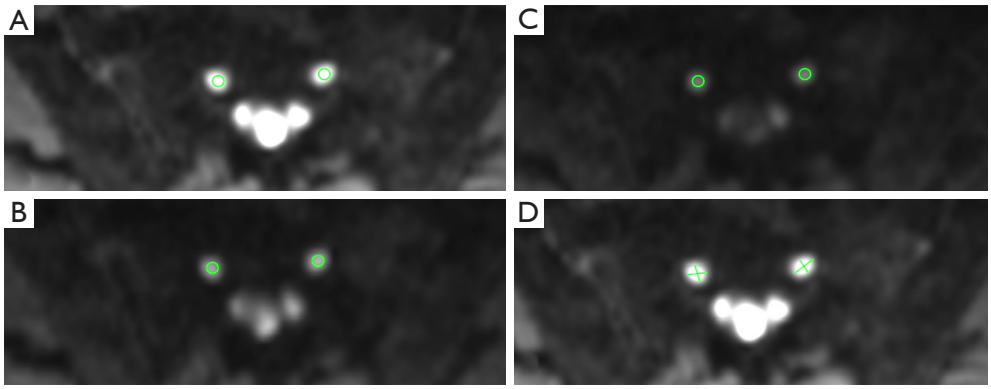

Figure 2 The green circles in diffusion weighted readout segmentation of long variable echo-trains (DW-RESOLVE) images (A) b=50, (B) b=500, (C) b=800 demonstrate examples of regions of interest (ROI) placements for S1 nerves. Image (D) b=50, the green dimensional calipers for size measurements.

(11 images for each b-value) were selected from the center of the phantom, and these images were used to measure the numerical indices of SNR and CNR. The SD was calculated using multiple slices.

Healthy volunteer imaging: Quantitative measurements were determined by calculating numerical values of MR image quality for the representative axial DWI-RESOLVE images through the lumbosacral nerves (L5, S1 and S2), which included: SNR and apparent diffusion coefficient (ADC) and nerve size using *Syngo* software (*Syngo*, Siemens Medical Solutions, Erlangen, Germany).

An expert MR radiographer measured the signal intensity to calculate the SNR and ADC values. Axial DWI-RESOLVE images were used to evaluate the lumbosacral nerves by precisely drawing ROIs within the center of the nerves (*Figure 2*), typically at a point approximately 3 cm distal to the exit foramen. The circular ROI sizes remained close to 5 mm^2 for all measurements. For SNR and ADC (b500 and b800) measurements, the ROIs were placed at the same spatial position for all b-value images to avoid bias (*Figure 2*). Furthermore, b-50 images were used for placing circular ROIs of the lumbosacral nerves as the signal intensity is greater and the shape of the nerves are well defined than b-500 and b-800 images. After that the ROI was copied to b-500 and b-800 images and each ROI was checked carefully that it is in the center of the nerve. For nerve size measurements, the AP and transverse dimensions of the lumbosacral nerves were assessed using the b-50 images as we found these modified evaluation of nerve root shape and size.

The SNR within the anatomical regions was calculated using the following formula (30):

$$SNR = SI_{(nerve)} / SD_{(noise)} \quad [1]$$

The $SI_{(nerve)}$ is signal intensity of the lumbosacral nerves, and $SD_{(noise)}$ is the standard deviation of the noise. A circular ROI within the image background was placed to measure the SD of the noise , avoiding any artifact if present.

The ADC values were calculated using the following formula (31):

$$ADC = \left[In\left(Sb0 / Sb1 \right) \right] / \left(b1 - b0 \right) \quad [2]$$

(*Sb0* = mean signal intensity for b-50 images, *Sb1*= mean signal intensity for b-500 or b-800 images, *b0*=50, and *b1*=500 or 800).

Qualitative assessment

Qualitative evaluation involved an independent, subjective evaluation of the degree of visibility of normal lumbosacral nerves and overall image quality. Assessment was performed by two musculoskeletal (MSK) radiologists, with 8 and 10 years of experience respectively, with images displayed on a PACS monitor with 5-megapixel resolution (*Barco*^{TM}). The standard lumbosacral 2D TSE images were evaluated by one radiologist to ensure that the volunteer participants did not have underlying disc herniation, spinal stenosis or other abnormality. Both readers independently evaluated the images acquired using the DWI-RESOLVE sequence.

Qualitative assessment included evaluation of the clarity of visualization of anatomical structures: L4, L5, S1, S2,

Table 2 Signal-to-noise ratio and contrast-to-noise ratio findings for the phantom images

Sequence type	SNR_{fluid}	SNR_{fat}	CNR
DWI-RESOLVE b-50	206.1 (±10.9)	23.1 (±10.6)	183 (±16.1)
DWI-RESOLVE b-500	125.1 (±45.2)	20.9 (±9.1)	107.3 (±42.7)
DWI-RESOLVE b-800	59.2 (±17.8)	20.2 (±7.7)	38.9 (±12.7)

Mean (± SD) of SNR and CNR shown by b-value. SNR, signal-to-noise ratio; CNR, contrast-to-noise ratio; DWI, diffusion weighted imaging; RESOLVE, readout segmentation of long variable echo-trains; SD, standard deviation.

S3, and sciatic nerves using an ordinal 5-point Likert-scale (1= not visible; 2= poor; 3= adequate; 4= good; 5= excellent) (32). Each anatomical structure was rated based on its appearance on DWI-RESOLVE images as follows: 1= no part of the nerve is visible (not visible); 2= nerve is barely, but incompletely visible; specifically, the distal part of the nerve is not visible (poor); 3= entire nerve is visible, including the proximal and distal parts, but these are incompletely visualized in a given image, or in a series of images (adequate); 4= entire nerve is visible, including the proximal and distal parts (good); 5= entire nerve is visible in its outline and extent within the slices acquired (excellent).

Furthermore, an ordinal 5-point Likert-scale was also employed to evaluate other aspects of the image quality, which included contrast between lumbosacral nerves and blood vessels, artifacts and noise (1= severe; 2= serious; 3= moderate; 4= minor; 5= none) (32,33). The severity of each type of artifact was subjectively graded as follows: 1= severe artifacts preventing visualization of the lumbosacral nerves (severe); 2= artifacts significantly reducing visibility of the lumbosacral nerves, resulting in serious impairment of diagnostic quality (serious); 3= clearly visible artifacts, resulting in partial visibility of the lumbosacral nerves; minimal acceptable image quality with some deficiencies (moderate); 4= barely visible artifacts, resulting in above average image quality, with minor deficiencies, which do not affect lumbosacral nerve visibility (minor); 5= no artifacts evident, with excellent visibility of the lumbosacral nerves (none) (32,33). The grading scales utilized for visualization of anatomical structures and image quality were piloted on images acquired from four healthy volunteers to ensure that the scales were appropriate for clinical use on the healthy volunteer cohort. At the time of each image evaluation session, the radiologists were blinded to the sequence parameters.

Statistical analysis

All statistical analyses were carried out using SPSS (IBM SPSS Statistics for Macintosh, Version 23.0, Armonk, NY: IBM Corp.). Statistical significance was assumed for $P<0.05$.

Phantom images: for phantom images, the distribution fitting each data set was assessed by obtaining descriptive statistics. SNR and CNR (mean and SD) were quantified for b-50, b-500 and b-800 images (*Table 2*).

Healthy volunteer imaging: The SNR, ADC and nerve size were compared using a Wilcoxon signed-rank test with Bonferroni correction. The SNR, ADC and nerve size (AP and transverse dimension) values for the right and left nerves were compared separately for each b-value. Due to repeated measurements collected on each patient, the Friedman test was used to test for differences in anatomical structure visualization, and image quality gradings across all b-values. The Friedman test is an omnibus test, and hence (when significant) was followed by pairwise *post hoc* testing using the Wilcoxon signed-rank test with Bonferroni correction. P-values reported therefore, are adjusted for multiple testing. Kappa (κ) statistics with 95% confidence intervals determined the inter and intra-observer agreement during MR image scoring. Specifically, κ is a measure of agreement beyond the level of agreement expected by chance alone and has a maximum value of one when there is perfect agreement and a minimum value of zero indicating no agreement (34).

Results

Quantitative data

Phantom

The SNR mean values for fluid and partially suppressed fat resulting from the DWI-RESOLVE sequence acquired with the three different b-values are listed in *Table 2*. In general, the SNR means for both fluid and fat were higher with the low b-value images. With respect to the contrast between fluid and fat, *Table 2* shows that it follows the previous results, as higher CNR means were associated with low b-values.

Healthy volunteers

The SNR, ADC and nerve size findings for normal lumbosacral nerves bilaterally had comparable values e.g., mean (± SD) SNR for S1 at b-50 images were 78.5 (±36.5) and 78.8 (±38.5) for the right and left sides, respectively

Table 3 Signal-to-noise ratio findings for lumbosacral nerves

Sequence type	L5		S1		S2	
	Right	Left	Right	Left	Right	Left
DWI-RESOLVE b-50	48.9 (±22.2)	48.9 (±21.0)	78.5 (±36.5)	78.8 (±38.5)	72.7 (±33.8)	75.2 (±32.8)
DWI-RESOLVE b-500	44.0 (±23.4)	44.4 (±21.4)	65.7 (±26.5)	70.4 (±29.4)	66.7 (±30.1)	69.7 (±32.2)
DWI-RESOLVE b-800	38.3 (±24.2)	38.9 (±23.7)	51.6 (±23.8)	54.2 (±25.2)	55.6 (±24.3)	59.4 (±29.4)

Mean (± SD) of SNR shown by DWI b-value and anatomical structure. Wilcoxon signed-rank tests were carried out comparing right and left, with P-value corrected for 9 tests, but no statistically significant differences were observed. DWI, diffusion weighted imaging; RESOLVE, readout segmentation of long variable echo-trains.

Table 4 Size measurements (mm) for lumbosacral nerves

Axis	L5		S1		S2	
	Right	Left	Right	Left	Right	Left
Vertical	5.7 (±0.1)	5.8 (±0.1)	6.0 (±0.1)	6.2 (±0.1)	5.6 (±0.1)	5.5 (±0.1)
Transverse	7.1 (±0.1)	7.2 (±0.1)	6.7 (±0.1)	6.8 (±0.1)	5.4 (±0.1)	5.3 (±0.1)

Mean (± SD) of nerve size shown by axis orientation and anatomical structure. Wilcoxon signed-rank tests were carried out comparing right and left, with P value corrected for 6 tests, but no statistically significant differences were observed. SD, standard deviation.

(*Tables 3*,*4* and *Figure 3*). Wilcoxon tests comparing SNR (acquired at each b-value), ADC and nerve size across normal right and left sided nerves for DWI-RESOLVE images were not significantly different for any anatomical structure (*Tables 3*,*4* and *Figure 3*). The SNR findings for b-50 images were higher than b-500 and b-800 images (*Table 3*).

Qualitative data

The findings of the MR images acquired using the routine lumbar spine protocol confirmed that all participants were healthy, with no evidence of bone, soft tissue or nerve abnormality involving the lumbosacral spine. *Table 5* summarizes the image scoring for clarity of visualization of anatomical structures, mean and SD for each lumbosacral nerve. In general, mean scores for clarity of visualization of these anatomical structures were found to be higher with DWI-RESOLVE b-50, followed by b-500 and b-800 images (*Figure 4*). Results for b-50 images were found to significantly differ when compared to b-800 images for all lumbosacral nerves except for S1 (P=0.055). The b-500 images were found to significantly differ relative to those for b-800 images for all lumbosacral nerves except for S3 (P=0.292).

Susceptibility artifact severity was approximately proportional to the higher b-value means of 4.3 (±0.8), 3.7 (±1.1) and 3.1 (±1.1) with b-50, b-500, and b-800, respectively (*Table 6*). In some of our cases, susceptibility artifact adversely affected the visualization of the lumbosacral nerves located at the margins of the defined FoV (*Figure 5*). While b-50 and b-500 images demonstrated higher SNR than b-800 images, the b-50 images were scored lower for the contrast between lumbosacral nerves and blood vessels (*Figure 6*). For contrast between lumbosacral nerves and blood vessels, reader-assigned scores for the b-50 images were found to differ significantly from those for the b-500 and b-800 images, with P=0.008 and P=0.009, respectively. However, for this image quality index, the b-500 images were not significantly different when compared to b-800 images.

While inter-observer agreement was moderate (0.41–0.60) for the grading of the b-800 images, substantial agreement (0.61–0.80) was associated with scoring of b-50 and b-500 images. Inter-observer agreement values and standard error were 0.81±0.04 (95% CI: 0.74–0.88), 0.77±0.04 (95% CI: 0.69–0.85), and 0.59±0.05 (95% CI: 0.49–0.69) for b-50, b-500, and b-800 images, respectively. Intra-observer agreement showed excellent agreement (0.81–1) within both readers across all b-value DWI-RESOLVE images (*Table 7*).

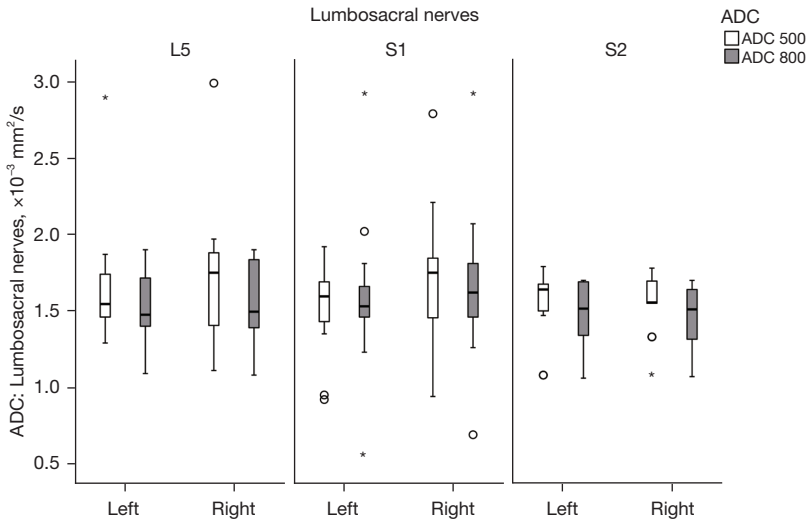

Figure 3 The relationship between ADC values and lumbosacral nerves sides for both ADC 500 and ADC 800. Circle = potential outlier, defined as value more than 1.5 interquartile above third quartile or below first quartile. Star = extreme value, more than 3 interquartiles above 3rd quartile or below 1st quartile. ADC, apparent diffusion coefficient.

Table 5 Anatomical structure visualization findings

Anatomical structures	DWI-RESOLVE b-50	DWI-RESOLVE b-500	DWI-RESOLVE b-800
L4	4.5 (±0.4)**	4.3 (±0.4)**	3.4 (±0.6)
L5	4.3 (±0.6)**	4.3 (±0.5)**	3.7 (±0.3)
S1	4.3 (±0.5)	4.6 (±0.4)**	3.8 (±0.4)
S2	4.1 (±0.7)**	4.4 (±0.7)**	3.4 (±0.5)
S3	3.1 (±0.6)**	2.9 (±0.8)	2.4 (±0.4)
SI	4.4 (±0.4)**	4.3 (±0.6)**	3.5 (±0.4)

Mean (± SD) of anatomical structure visualization shown by DWI b-value and anatomical structure, and p-values from Wilcoxon signed-rank tests were corrected for 24 tests. *, Bonferroni-adjusted P value <0.05 when DWI-RESOLVE b-50 is compared to DWI-RESOLVE b-500. **, Bonferroni-adjusted P value <0.05 when DWI-RESOLVE b-50 or DWI-RESOLVE b-500 is compared to DWI-RESOLVE b-800. DWI, diffusion weighted imaging; RESOLVE, readout segmentation of long variable echo-trains; SD, standard deviation.

Discussion

While studies evaluating the DWI-RESOLVE sequence are reported in the literature (16-21), to our knowledge, no published studies evaluating the use of this sequence for the assessment of lumbosacral nerve abnormalities such as those associated with nerve irritation due to stenosis and/or discogenic disease of the lumbar spine could be sourced. Previous studies have focused on the applications of DWI-RESOLVE in different parts of the body such as the musculoskeletal system (17), kidneys (20), breast (21,22), brain (23), prostate gland (35), pelvic tumors (36), and pelvic splanchnic nerve (37).

Several studies have determined the utility of ss-EPI DWI in the musculoskeletal system and lumbosacral nerves (11,12,17). However, the severity of inherent geometric distortion, signal loss and T2* blurring, particularly at the air-, bone-soft tissue boundaries encountered when imaging the lumbosacral region has the potential to limit the utility of ss-EPI DWI for accurate nerve size measurement to differentiate normality from compression-induced inflammation. These adverse image quality effects are augmented at 3T, requiring parameter modification.

Technological advances in scanner hardware and software

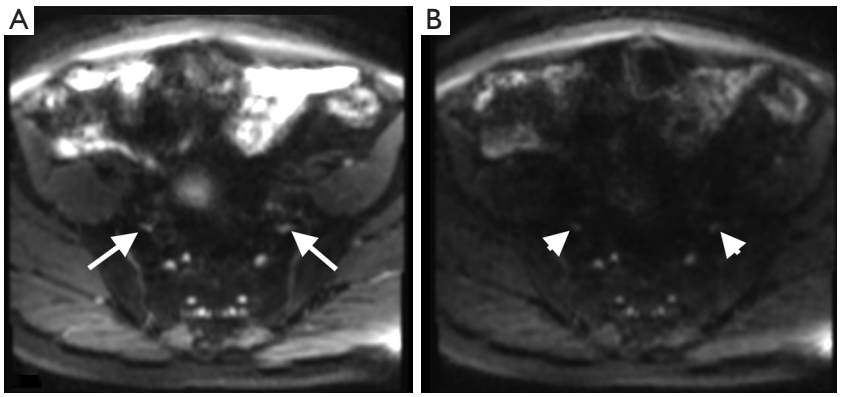

Figure 4 Axial DW-RESOLVE images for a 51-year-old female healthy volunteer highlighting the visualization performance for the lumbosacral nerves. While L5 nerves (arrows) were well visualized with b-50 images (A), L5 nerves (arrow heads) were poorly visualized with b-800 images (B). The signal intensity and therefore the conspicuity of the sacral nerves is slightly reduced in (B). DW-RESOLVE, diffusion weighted readout segmentation of long variable echo-trains.

Table 6 Image quality scores for DWI-RESOLVE images

Image quality	DWI-RESOLVE b-50	DWI-RESOLVE b-500	DWI-RESOLVE b-800
Susceptibility artifact	4.3 (±0.8)*/**	3.7 (±1.1)**	3.1 (±1.1)
Noise	3.8 (±0.3)**	3.8 (±0.3)**	3.2 (±0.4)
CNR lumbosacral nerves/blood vessels	2.3 (±0.5)*/**	3.0 (±0.2)	3.1 (±0.4)

Mean (± SD) of image quality shown by DWI b-value and image quality criteria, and P values from Wilcoxon signed-rank tests were corrected for 12 tests. *, Bonferroni-adjusted P value 0.05 when DWI-RESOLVE b-50 is compared to DWI-RESOLVE b-500. **, Bonferroni-adjusted P value <0.05 when DWI-RESOLVE b-50 or DWI-RESOLVE b-500 is compared to DWI-RESOLVE b-800. DWI, diffusion weighted imaging; RESOLVE, readout segmentation of long variable echo-trains; CNR, contrast-to-noise ratio; SD, standard deviation.

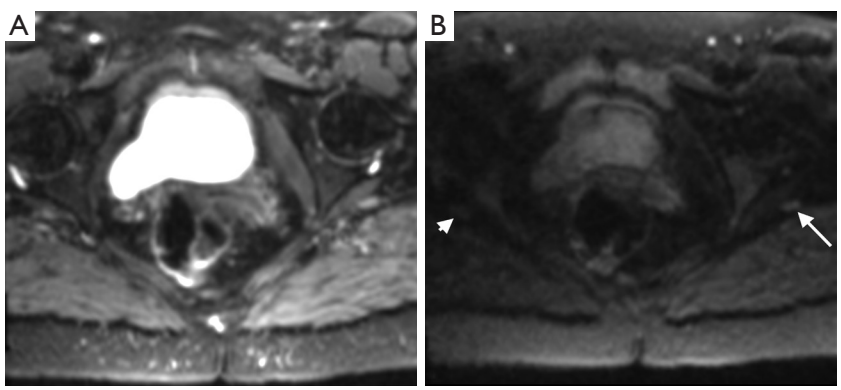

Figure 5 Axial DW-RESOLVE images of lumbosacral region in a healthy volunteer (A) b=50 and (B) b=800 demonstrating the effect of susceptibility artifact. The susceptibility effect was minor and slight signal loss was evident in the right side compared to the left (A). The image demonstrates moderate loss of signal on the right side of the body compared to the left (B). The right sciatic nerve (arrow head) is hypointense relative to the sciatic nerve (arrow) in the left side. The normal left sciatic nerve (arrow) appears asymmetric due to this spurious artifact. DW-RESOLVE, diffusion weighted readout segmentation of long variable echo-trains.

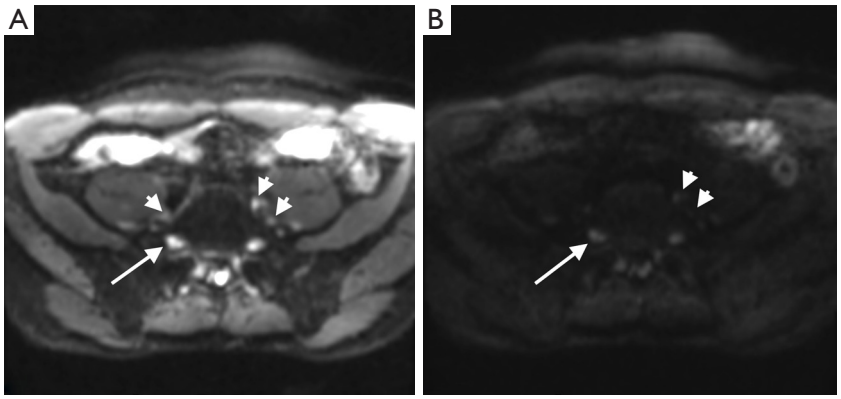

Figure 6 Axial DW-RESOLVE images for a 32-year-old female healthy volunteer demonstrating the contrast between lumbosacral nerves and blood vessels. The contrast between right L5 nerve root (arrows) and adjacent blood vessels (arrow heads) was poor with DWI-RESOLVE b-50 image (A). The contrast between L5 (arrows) and blood vessels (arrow heads) was excellent with DW-RESOLVE b-800 image as flowing blood vessel generated hypointense signal compared to the L5 nerves (B). DW-RESOLVE, diffusion weighted readout segmentation of long variable echo-trains.

Table 7 Intra-observer agreement findings for both readers

Sequence type	Reader 1		Reader 2	
	κ ± SE	95% CI	κ ± SE	95% CI
DWI-RESOLVE b-50	0.83±0.14	0.55, 1.1	0.83±0.11	0.62, 1
DWI-RESOLVE b-500	0.92±0.08	0.76, 1.1	0.83±0.11	0.62, 1
DWI-RESOLVE b-800	0.83±0.1	0.6, 1.1	0.82±0.1	0.58, 1

CI, confidence interval; SE, standard error; DWI, diffusion weighted imaging; RESOLVE, readout segmentation of long variable echo-trains.

have facilitated readout-segmented EPI DWI, for which a reduction in the number of columns in the readout direction supports fast gradient reversals, in turn reducing echo-spacing, overall readout time and susceptibility artifacts (16,17,19). The shorter spacing between echoes in the echo train further reduces geometric distortion, T2* blurring and susceptibility artifacts (37). While these characteristics of the readout segmented EPI DWI-RESOLVE sequence provide potential for improvements in image quality through fewer artifacts, reduced signal loss and higher spatial resolution, to our knowledge, these features have not been described for the lumbosacral nerves. Therefore, this study involved the evaluation of the technical quality of 3T DWI-RESOLVE images of a phantom and the lumbosacral nerves of healthy volunteers in preparation for clinical study (26), with opportunities for improving the visibility of lumbosacral nerves and image quality.

The non-modified DWI-RESOLVE sequence was originally designed for evaluating the prostate gland, which, as a small anatomical structure, can be encompassed using a smaller FoV and fewer slices. The more extensive anatomical coverage required to evaluate the lumbosacral nerves necessitated an appreciable increase in TR, which, while enabling the number of slices to be doubled, in turn lengthened the acquisition time.

This modification and subsequent evaluation of the DWI-RESOLVE sequence was required due to the small size of the lumbosacral nerves and their anatomical location surrounded by different tissue interfaces including soft tissue/bone interfaces in the lumbar spine and tissue/air interfaces in the bowel, which may degrade the image quality (11,38,39).

The two regions method was utilized to calculate SNR as this technique was found to be more practical, especially for human subject imaging with sequences that require relatively long acquisition times such as the EPI DWI-RESOLVE (26). While the subtraction method for SNR calculation is reported to be more accurate and robust (40), it is impractical for human subject imaging as it requires each sequence to be acquired twice, increasing the likelihood that signal variations may occur due to patient motion and physiological effects, thereby introducing a potential for differences in SNR values due to these sources of error (41).

Eguchi *et al.* (11,14), used the ADC map images to calculate ADC for b-1,000 images; however, this technique is reported to be unreliable as mis-registration between b-0 and the other b-value images usually arises as a result of image distortion from motion probing gradients (13,42). The limitation of this technique became more pronounced when calculating ADC values for small regions such as nerves, with the potential to generate inaccurate information (13). A further method relies on using different b-value images to calculate the ADC values (31,42) and was used in our study based on the evidence for its robustness and more accurate ADC values.

Previous studies used b-values of 0 and 1,000 s/mm^2 with ss-EPI-DWI images for the evaluation of lumbosacral nerves (11,13,14). A recent study evaluated the sciatic nerve using 16 b values ranged from 0–1,500 s/mm^2 (43). Our modified DWI-RESOLVE sequence included three different b-values 50, 500 and 800 s/mm^2. These values reflect low, intermediate, and high b-values. We found these b-values to be more favorable for the DWI-RESOLVE sequence. During preliminary modification phase DWI-RESOLVE imaging, we found the SNR of the lumbosacral plexus could be suboptimal at a b-value of 1,000 s/mm^2 but reasonable at a b-value of 800 s/mm^2. Expert radiologists determined that the b-50 images were best for evaluating the shape and size of nerves and the b-500 and b-800 images were more appropriate for assessing signal intensity together with high contrast between the lumbosacral nerves and blood vessels. We found that the resultant poor contrast resolution between lumbosacral nerves and blood vessels tended to prolong the evaluation of the nerves during both the objective and subjective measurement processes.

A number of study limitations are recognized. The participants of this study were all healthy, and the MR signal intensity values for the lumbosacral nerves may change under disease conditions. However, this experimental phase involving normal lumbar spinal nerve imaging was considered necessary to ensure that the DWI-RESOLVE sequence produced images of sufficient quality to enable radiologists to visualize the small-diameter normal lumbosacral nerves before applying the sequence on a patient cohort. While the long scan time for DWI-RESOLVE creates potential for motion-related artifact in restless patients, further technical advances in sequence design, including simultaneous multi-slice imaging such recent may help to offset this penalty (44). The quantitative values for S3 and the blood vessels were not included as these anatomical structures were too small in diameter for ROI placement. The justification for omitting these measurements is supported in a study by Eguchi *et al.* (14) who suggested that ROIs should be smaller than the anatomical structures being evaluated to avoid partial volume averaging effect. A further potential limitation of our study is that, despite the radiologists being blinded to the DWI b-values, the DWI b-value images with signal intensity characteristics that were recognizable for each b-value to the reviewing radiologists. However, this bias is unavoidable and was not considered to adversely impact on quality scoring by the radiologists. Only the axial plane DWI-RESOLVE images were acquired as the research team found that this plane was more appropriate to evaluate the lumbosacral nerves in terms of performing quantitative and qualitative assessments and measurements of the transverse and vertical axes of each nerve, a strategy that was followed by other researchers (13).

In conclusion, the phantom and volunteer experimental phases of this study were undertaken to ensure that the image quality associated with the locally modified DWI-RESOLVE MR pulse sequence was clinically verified prior to utilizing it on patients with suspected lumbosacral nerve abnormalities. The resultant DWI-RESOLVE images were of a quality that facilitated visualization of the normal lumbosacral nerves with acceptable image quality. These findings support the clinical applicability of this sequence. While the DWI-RESOLVE sequence has now been integrated into the lumbar spine MR scanning protocol, continued technological developments in pulse sequence design will contribute further improvements in acquisition time, SNR and spatial resolution

Acknowledgments

The authors acknowledge the support provided by the Radiology Department at the Mater Misericordiae University Hospital in Dublin.
Funding: None.

Footnote

Reporting Checklist: The authors have completed the MDAR reporting checklist. Available at https://qims.amegroups.com/article/view/10.21037/qims-22-191/rc

Conflicts of Interest: All authors have completed the ICMJE uniform disclosure form (available at https://qims.amegroups.com/article/view/10.21037/qims-22-191/coif).

The authors have no conflicts of interest to declare.

Ethical Statement: The authors are accountable for all aspects of the work in ensuring that questions related to the accuracy or integrity of any part of the work are appropriately investigated and resolved. The study was conducted in accordance with the Declaration of Helsinki (as revised in 2013). Ethical approval was obtained prior to commencing phantom and healthy volunteers recruitment and scanning. This research study was approved by the Research Ethics Committee at the Mater Misericordiae University Hospital, Dublin, Ireland (Reference number: 1/378/1719). Written consent form was obtained from all the participants before the MRI examinations.

References

1. Macintosh BJ, Graham SJ. Magnetic resonance imaging to visualize stroke and characterize stroke recovery: a review. Front Neurol 2013;4:60.
2. Cihangiroglu M, Citci B, Kilickesmez O, Firat Z, Karlıkaya G, Uluğ AM, Bingol CA, Kovanlikaya I. The utility of high b-value DWI in evaluation of ischemic stroke at 3T. Eur J Radiol 2011;78:75-81.
3. Smajlović D, Sinanović O. Sensitivity of the neuroimaging techniques in ischemic stroke. Med Arh 2004;58:282-4.
4. Lansberg MG, Norbash AM, Marks MP, Tong DC, Moseley ME, Albers GW. Advantages of adding diffusion-weighted magnetic resonance imaging to conventional magnetic resonance imaging for evaluating acute stroke. Arch Neurol 2000;57:1311-6.
5. Yu Y, Zhang H, Xiao Z, She D, Xing Z, Yang X, Cao D. Diffusion-weighted MRI combined with susceptibility-weighted MRI: added diagnostic value for four common lateral ventricular tumors. Acta Radiol 2018;59:980-7.
6. Lai PH, Chung HW, Chang HC, Fu JH, Wang PC, Hsu SH, Hsu SS, Lin HS, Chuang TC. Susceptibility-weighted imaging provides complementary value to diffusion-weighted imaging in the differentiation between pyogenic brain abscesses, necrotic glioblastomas, and necrotic metastatic brain tumors. Eur J Radiol 2019;117:56-61.
7. Bharwani N, Koh DM. Diffusion-weighted imaging of the liver: an update. Cancer Imaging 2013;13:171-85.
8. Taouli B, Koh DM. Diffusion-weighted MR imaging of the liver. Radiology 2010;254:47-66.
9. Taouli B, Thakur RK, Mannelli L, Babb JS, Kim S, Hecht EM, Lee VS, Israel GM. Renal lesions: characterization with diffusion-weighted imaging versus contrast-enhanced MR imaging. Radiology 2009;251:398-407.
10. Khoo MM, Tyler PA, Saifuddin A, Padhani AR. Diffusion-weighted imaging (DWI) in musculoskeletal MRI: a critical review. Skeletal Radiol 2011;40:665-81.
11. Eguchi Y, Ohtori S, Yamashita M, Yamauchi K, Suzuki M, Orita S, Kamoda H, Arai G, Ishikawa T, Miyagi M, Ochiai N, Kishida S, Inoue G, Masuda Y, Ochi S, Kikawa T, Toyone T, Takaso M, Aoki Y, Takahashi K. Diffusion-weighted magnetic resonance imaging of symptomatic nerve root of patients with lumbar disk herniation. Neuroradiology 2011;53:633-41.
12. Reinhold M, Ederer C, Henninger B, Eberwein A, Kremser C. Diffusion-weighted magnetic resonance imaging for the diagnosis of patients with lumbar nerve root entrapment syndromes: results from a pilot study. Eur Spine J 2015;24:319-26.
13. Takashima H, Takebayashi T, Yoshimoto M, Terashima Y, Ida K, Yamashita T. Efficacy of diffusion-weighted magnetic resonance imaging in diagnosing spinal root disorders in lumbar disc herniation. Spine (Phila Pa 1976) 2013;38:E998-1002.
14. Eguchi Y, Ohtori S, Yamashita M, Yamauchi K, Suzuki M, Orita S, Kamoda H, Arai G, Ishikawa T, Miyagi M, Ochiai N, Kishida S, Masuda Y, Ochi S, Kikawa T, Takaso M, Aoki Y, Toyone T, Suzuki T, Takahashi K. Clinical applications of diffusion magnetic resonance imaging of the lumbar foraminal nerve root entrapment. Eur Spine J 2010;19:1874-82.
15. Kanamoto H, Eguchi Y, Oikawa Y, Orita S, Inage K, Fujimoto K, Shiga Y, Abe K, Inoue M, Kinoshita H, Matsumoto K, Masuda Y, Furuya T, Koda M, Aoki Y, Watanabe A, Takahashi K, Ohtori S. Visualization of lumbar nerves using reduced field of view diffusion tensor imaging in healthy volunteers and patients with degenerative lumbar disorders. Br J Radiol 2017;90:20160929.
16. Porter DA, Heidemann RM. High resolution diffusion-weighted imaging using readout-segmented echo-

planar imaging, parallel imaging and a two-dimensional navigator-based reacquisition. Magn Reson Med 2009;62:468-75.
17. Zhang H, Huang H, Zhang Y, Tu Z, Xiao Z, Chen J, Cao D. Diffusion-Weighted MRI to Assess Sacroiliitis: Improved Image Quality and Diagnostic Performance of Readout-Segmented Echo-Planar Imaging (EPI) Over Conventional Single-Shot EPI. AJR Am J Roentgenol 2021;217:450-9.
18. Frost R, Jezzard P, Douaud G, Clare S, Porter DA, Miller KL. Scan time reduction for readout-segmented EPI using simultaneous multislice acceleration: Diffusion-weighted imaging at 3 and 7 Tesla. Magn Reson Med 2015;74:136-49.
19. Yeom KW, Holdsworth SJ, Van AT, Iv M, Skare S, Lober RM, Bammer R. Comparison of readout-segmented echo-planar imaging (EPI) and single-shot EPI in clinical application of diffusion-weighted imaging of the pediatric brain. AJR Am J Roentgenol 2013;200:W437-43.
20. Friedli I, Crowe LA, Viallon M, Porter DA, Martin PY, de Seigneux S, Vallée JP. Improvement of renal diffusion-weighted magnetic resonance imaging with readout-segmented echo-planar imaging at 3T. Magn Reson Imaging 2015;33:701-8.
21. Wisner DJ, Rogers N, Deshpande VS, Newitt DN, Laub GA, Porter DA, Kornak J, Joe BN, Hylton NM. High-resolution diffusion-weighted imaging for the separation of benign from malignant BI-RADS 4/5 lesions found on breast MRI at 3T. J Magn Reson Imaging 2014;40:674-81.
22. Bogner W, Pinker-Domenig K, Bickel H, Chmelik M, Weber M, Helbich TH, Trattnig S, Gruber S. Readout-segmented echo-planar imaging improves the diagnostic performance of diffusion-weighted MR breast examinations at 3.0 T. Radiology 2012;263:64-76.
23. Holdsworth SJ, Yeom K, Skare S, Gentles AJ, Barnes PD, Bammer R. Clinical application of readout-segmented-echo-planar imaging for diffusion-weighted imaging in pediatric brain. AJNR Am J Neuroradiol 2011;32:1274-9.
24. Yoshimura Y, Kuroda M, Sugiantoc I, Bamgbosec BO, Miyahara K, Ohmura Y, Kurozumi A, Matsushita T, Ohno S, Kanazawa S, Asaumi J. The Usefulness of Readout-Segmented Echo-Planar Imaging (RESOLVE) for Bio-phantom Imaging Using 3-Tesla Clinical MRI. Acta Med Okayama 2018;72:53-9.
25. Xu X, Wang Y, Hu H, Su G, Liu H, Shi H, Wu F. Readout-segmented echo-planar diffusion-weighted imaging in the assessment of orbital tumors: comparison with conventional single-shot echo-planar imaging in image quality and diagnostic performance. Acta Radiol 2017;58:1457-67.
26. Abdulaal OM, McGee A, Rainford L, O'Driscoll D, Galligan M, Reid V, MacMahon PJ. Identifying lumbosacral plexus nerve root abnormalities in patients with sciatica using 3T readout-segmented echo-planar diffusion weighted MR neurography. Insights Imaging 2021;12:54.
27. Winfield JM, Douglas NH, deSouza NM, Collins DJ. Phantom for assessment of fat suppression in large field-of-view diffusion-weighted magnetic resonance imaging. Phys Med Biol 2014;59:2235-48.
28. Kanal E, Barkovich AJ, Bell C, Borgstede JP, Bradley WG Jr, Froelich JW, et al. ACR guidance document for safe MR practices: 2007. AJR Am J Roentgenol 2007;188:1447-74.
29. Zhang Z, Song L, Meng Q, Li Z, Pan B, Yang Z, Pei Z. Morphological analysis in patients with sciatica: a magnetic resonance imaging study using three-dimensional high-resolution diffusion-weighted magnetic resonance neurography techniques. Spine (Phila Pa 1976) 2009;34:E245-50.
30. Yoneyama M, Takahara T, Kwee TC, Nakamura M, Tabuchi T. Rapid high resolution MR neurography with a diffusion-weighted pre-pulse. Magn Reson Med Sci 2013;12:111-9.
31. Demir OI, Obuz F, Sağol O, Dicle O. Contribution of diffusion-weighted MRI to the differential diagnosis of hepatic masses. Diagn Interv Radiol 2007;13:81-6.
32. Sutter R, Hodek R, Fucentese SF, Nittka M, Pfirrmann CW. Total knee arthroplasty MRI featuring slice-encoding for metal artifact correction: reduction of artifacts for STIR and proton density-weighted sequences. AJR Am J Roentgenol 2013;201:1315-24.
33. Tagliafico A, Bignotti B, Tagliafico G, Martinoli C. Usefulness of IDEAL T2 imaging for homogeneous fat suppression and reducing susceptibility artefacts in brachial plexus MRI at 3.0 T. Radiol Med 2016;121:45-53.
34. Landis JR, Koch GG. The measurement of observer agreement for categorical data. Biometrics 1977;33:159-74.
35. Zhang YD, Wu CJ, Bao ML, Li H, Yan X, Liu XS, Shi HB. New RESOLVE-Based Diffusional Kurtosis Imaging in MRI-Visible Prostate Cancer: Effect of Reduced b Value on Image Quality and Diagnostic Effectiveness. AJR Am J Roentgenol 2016;207:330-8.
36. Foltz WD, Porter DA, Simeonov A, Aleong A, Jaffray D, Chung P, Han K, Ménard C. Readout-segmented echo-planar diffusion-weighted imaging improves geometric

performance for image-guided radiation therapy of pelvic tumors. Radiother Oncol 2015;117:525-31.
37. Yamashita R, Isoda H, Arizono S, Furuta A, Ohno T, Ono A, Murata K, Togashi K. Selective visualization of pelvic splanchnic nerve and pelvic plexus using readout-segmented echo-planar diffusion-weighted magnetic resonance neurography: A preliminary study in healthy male volunteers. Eur J Radiol 2017;86:52-7.
38. Cejas C, Escobar I, Serra M, Barroso F. High resolution neurography of the lumbosacral plexus on 3T magneteic resonance imaging. Radiologia 2015;57:22-34.
39. Yang RK, Roth CG, Ward RJ, deJesus JO, Mitchell DG. Optimizing abdominal MR imaging: approaches to common problems. Radiographics 2010;30:185-99.
40. Notohamiprodjo M, Horng A, Kuschel B, Paul D, Li G, Raya JG, Reiser MF, Glaser C. 3D-imaging of the knee with an optimized 3D-FSE-sequence and a 15-channel knee-coil. Eur J Radiol 2012;81:3441-9.
41. Dietrich O, Raya JG, Reeder SB, Reiser MF, Schoenberg SO. Measurement of signal-to-noise ratios in MR images: influence of multichannel coils, parallel imaging, and reconstruction filters. J Magn Reson Imaging 2007;26:375-85.
42. Ichikawa T, Haradome H, Hachiya J, Nitatori T, Araki T. Diffusion-weighted MR imaging with single-shot echo-planar imaging in the upper abdomen: preliminary clinical experience in 61 patients. Abdom Imaging 1999;24:456-61.
43. Foesleitner O, Sulaj A, Sturm V, Kronlage M, Godel T, Preisner F, Nawroth PP, Bendszus M, Heiland S, Schwarz D. Diffusion MRI in Peripheral Nerves: Optimized b Values and the Role of Non-Gaussian Diffusion. Radiology 2022;302:153-61.
44. Filli L, Ghafoor S, Kenkel D, Liu W, Weiland E, Andreisek G, Frauenfelder T, Runge VM, Boss A. Simultaneous multi-slice readout-segmented echo planar imaging for accelerated diffusion-weighted imaging of the breast. Eur J Radiol 2016;85:274-8.

Cite this article as: Abdulaal OM, MacMahon PJ, Rainford L, Cradock A, O'Driscoll D, Galligan M, Alshoabi SA, Alsharif W, McGee A. Evaluation of image quality of diffusion weighted readout segmentation of long variable echo-trains MR pulse sequence for lumbosacral nerve imaging at 3T. Quant Imaging Med Surg 2023;13(1):196-209. doi: 10.21037/qims-22-191

